Spin-independent elastic WIMP scattering and the DAMA annual modulation signal

Malcolm Fairbairn[a,b] and Thomas Schwetz[a]

[a]Physics Department, Theory Division, CERN,
  1211 Geneva 23, Switzerland

[b]King's College London,
  Strand, WC2R 2LS, U.K.

E-mail: malc@cern.ch, schwetz@cern.ch

Abstract. We discuss the interpretation of the annual modulation signal seen in the DAMA experiment in terms of spin-independent elastic WIMP scattering. Taking into account channeling in the crystal as well as the spectral signature of the modulation signal we find that the low-mass WIMP region consistent with DAMA data is confined to WIMP masses close to $m_\chi \simeq 12\,\mathrm{GeV}$, in disagreement with the constraints from CDMS and XENON. We conclude that even if channeling is taken into account this interpretation of the DAMA modulation signal is disfavoured. There are no overlap regions in the parameter space at 90% CL and a consistency test gives the probability of 1.2×10^{-5}. We study the robustness of this result with respect to variations of the WIMP velocity distribution in our galaxy, by changing various parameters of the distribution function, and by using the results of a realistic N-body dark matter simulation. We find that only by making rather extreme assumptions regarding halo properties can we obtain agreement between DAMA and CDMS/XENON.

JCAP01(2009)037

Contents

1   Introduction

The DAMA collaboration has collected an impressive amount of data in their search for the scattering of weakly interacting dark matter particles (WIMPs) off Sodium Iodine. The combined data from DAMA/NaI (7 annual cycles) and DAMA/LIBRA (4 annual cycles) amounts to a total exposure of 0.82 ton yr [1], in a field where exposure is measured in units of kg days. DAMA/LIBRA has now provided further evidence for an annual modulation of the event rate in the energy range between 2 and 6 keVee, the claimed statistical confidence of the positive signal being 8.2σ [1]. The phase of the observed modulation (with maximum on day 144 ± 8) is in striking agreement with the expectation for a modulation in a WIMP scattering signal due to the rotation of the Earth around the Sun, (expected maximum day 152, June 2nd), see e.g., [2] for a review. An interpretation of this effect in terms of spin-independent interactions of conventional WIMPs with masses $m_\chi \gtrsim 50\,\text{GeV}$ is in direct conflict with the constraints from several experiments looking for direct WIMP detection, most notably with the data from CDMS [3] and XENON10 [4], which exclude the WIMP cross section consistent with the DAMA modulation for $m_\chi \sim 50\,\text{GeV}$ by many orders of magnitude. In light of this, several alternative explanations of the DAMA annual modulation have been proposed, for example spin-dependent interactions [5, 6], light WIMPs with $\lesssim 10\,\text{GeV}$ masses [7–9], keV scale axion-like dark matter [10] (see however, [11, 12]), dark matter interacting only with electrons [13], inelastic WIMP scattering [14, 15] and mirror dark matter [16].

In this work we reconsider the possibility of spin-independent elastic scattering of light WIMPs with $\lesssim 10\,\text{GeV}$ masses [7–9], see [17–20] for recent studies. The original idea is that light dark matter scattering on the relatively light Sodium nuclei in DAMA could deposit enough energy in the detector to give a signal, whereas the scattering of light halo particles off heavier nuclei, such as for example Ge in CDMS or Xe in XENON would lead to energy

depositions below the threshold of those detectors. Recently the importance of the so-called channeling effect [21] in the crystal structure of the experiment has also been emphasized [18, 19]. Specific models for WIMPs with $m_\chi \sim 10\,\mathrm{GeV}$ have been studied for example in [17, 22–24]. Here we do not discuss theoretical implications but focus on the phenomenology of direct detection experiments in a model-independent way by assuming that such light WIMPs can provide the correct relic abundance while any direct collider constraints can be evaded.

In this region of WIMP masses several experiments [25–28] exclude WIMP-nucleon scattering cross sections in the range $\sigma_p \gtrsim 10^{-40}$ cm^2. As we will see in the next pages, once we have included channeling as well as the spectral shape of the DAMA modulation signal, the allowed region of our interest is obtained at much small cross sections, around $\sigma_p \sim 10^{-41}$ cm^2 and $m_\chi \sim 10\,\mathrm{GeV}$. In this region the most relevant constraints come from XENON [4], the 2008 Germanium data from CDMS [3], and the 2005 CDMS data on Silicon [29]. Indeed, as we will discuss, the spectral shape of the DAMA annual modulation restricts m_χ and σ_p to a region excluded by these experiments.

In our study we elaborate on this result and discuss how robust it is with respect to different assumptions about the dark matter halo of our galaxy. The impact of non-standard halo properties on dark matter direct detection experiments has been discussed by many authors, see for example [30–33]. At a qualitative level, one would expect that smaller velocity dispersions or truncated velocity distributions would seem to favour the dark matter interpretation of the DAMA signal, as they could lead to more events above the low energy threshold of DAMA but below that of other experiments. Furthermore, anisotropies in the velocity dispersion could amplify annual modulation signals.

The outline of our work is as follows. In section 2 we briefly summarise the phenomenology of elastic WIMP scattering in direct detection experiments and give some technical details on our analysis of DAMA, CDMS and XENON data. The results for a standard dark matter halo are presented in section 3. In section 4 we consider deviations from the standard assumptions made about the WIMP velocity distribution: we use results from the Via Lactea N-body dark matter simulation [34], we vary several parameters of the Maxwellian distribution and consider asymmetric velocity profiles. Section 5 contains our conclusions. In appendix A we comment on the DAMA fit using the annual modulation energy spectrum, and in appendix B we briefly compare our results to the ones from other authors.

2 The WIMP signal in direct detection experiments

In this section we briefly summarise the phenomenology of WIMP scattering and describe our analysis of DAMA, CDMS and XENON data.

2.1 The event spectrum from elastic WIMP scattering

The differential event spectrum for WIMP scattering in counts per unit mass of a given nucleus per unit exposure time and per unit energy as a function of the recoil energy E_R is given by the expression (see e.g., [2])

$$R(E_R) = \frac{\rho\,\sigma_p A^2 F^2(q)}{2m_\chi \mu_p^2}\,\eta(E_R, t)\,. \tag{2.1}$$

Here ρ is the local WIMP energy density for which we adopt the canonical value $\rho = 0.3\,\mathrm{GeV/cm^3}$, σ_p is the WIMP scattering cross section on a proton,[1] A is the mass number of the target nucleus, $\mu_p = m_\chi m_p/(m_\chi + m_p)$ is the reduced WIMP-proton mass and we use the common Helm form factor $F(q) = 3e^{-q^2 s^2/2}[\sin(qr) - qr\cos(qr)]/(qr)^3$, with $s = 1$ fm, $r = \sqrt{R^2 - 5s^2}$, $R = 1.2A^{1/3}$ fm, $q = \sqrt{2ME_R}$, with M being the nucleus mass. The function η contains the integral over the WIMP velocity distribution:

$$\eta(E_R, t) = \int d\Omega_{\mathbf{v}} \int_{v_{\min}(E_R)}^{\infty} dv\, v\, f_\oplus(\mathbf{v}, t)\,, \qquad (2.2)$$

where $v_{\min} = \sqrt{ME_R/2\mu_M^2}$ is the minimum velocity of a WIMP to produce a recoil energy E_R, and $v = |\mathbf{v}|$. The WIMP velocity distribution in the Earth rest frame $f_\oplus(\mathbf{v}, t)$ is obtained from the distribution in the galactic rest frame $f_{\mathrm{gal}}(\mathbf{v})$ by

$$f_\oplus(\mathbf{v}, t) = f_{\mathrm{gal}}(\mathbf{v} + \mathbf{v}_\odot + \mathbf{v}_\oplus(t))\,. \qquad (2.3)$$

In the coordinate system in which x points towards the galactic center, y towards the direction of galactic rotation, and z towards the galactic north pole, we use for the velocity of the Sun $\mathbf{v}_\odot = (0, 220, 0) + (10, 13, 7)$ km/s [35] (including the local Keplerian velocity of 220 km/s [36] as well as the Sun's peculiar velocity, see also [37] and references therein). To describe the motion of the Earth around the Sun we use the parametrisation of [35]: $\mathbf{v}_\oplus(t) = v_\oplus(\mathbf{e}_1 \sin\lambda - \mathbf{e}_2 \cos\lambda)$, with $v_\oplus = 2\pi\mathrm{A.U.}/\mathrm{yr} = 29.8$ km/s, $\mathbf{e}_1 = (-0.0670, 0.4927, -0.8676)$, $\mathbf{e}_2 = (-0.9931, -0.1170, 0.01032)$, and $\lambda(t) = 2\pi(t - 0.218)$.

The "standard halo model" assumes for the DM distribution an isotropic isothermal sphere, which leads to a Maxwellian velocity distribution in the galactic frame, truncated at the escape velocity v_{esc}:

$$f_{\mathrm{gal}}(\mathbf{v}) = \begin{cases} N\left[\exp\left(-v^2/\bar{v}^2\right) - \exp\left(-v_{\mathrm{esc}}^2/\bar{v}^2\right)\right] & v < v_{\mathrm{esc}} \\ 0 & v > v_{\mathrm{esc}} \end{cases}\,, \qquad (2.4)$$

where we adopt as default values $\bar{v} = 220$ km/s and $v_{\mathrm{esc}} = 650$ km/s. Here and throughout the paper we use the notation $\bar{v}^2 = 2(<v^2> - <v>^2) = 2\sigma^2$. In order to properly take into account the impact of the finite escape velocity as well as allowing for non-standard halos deviating from eq. (2.4) we perform the integral in eq. (2.2) numerically. In section 3 we first consider the standard halo model, whereas in section 4 we go beyond these default assumptions by varying the parameters of the velocity distribution as well as changing its shape.

2.2 On quenching and channeling

In the analysis of DAMA data the effects of quenching and channeling are important [21, 38]. For quenched events the recoiling nucleus loses its energy both electromagnetically as well as via nuclear force interactions, where the light yield in the scintillator comes mainly from the electromagnetic part. To take this effect into account the event energy is measured in equivalent electron energy (in keVee), defined by $q \times E_R$ for the total nuclear recoil energy E_R in keV. For the elements in DAMA one has $q_{\mathrm{Na}} = 0.3$ and $q_{\mathrm{I}} = 0.09$. However, due to the crystalline structure of the target, for certain angles and energies of the particles no nuclear force interactions happen and the entire energy is lost electromagnetically. Hence, for these

---

[1]Note that only the product of $\rho \times \sigma_p$ is relevant for the scattering rate. Therefore, whenever we use the symbol σ_p the cross section is implicitly normalised to the value of $\rho = 0.3\,\mathrm{GeV/cm^3}$.

so-called channeled events one has $q \approx 1$, see [21, 38]. For the fraction f of channeled events relevant for DAMA we use the parameterisation

$$f_{\mathrm{Na}}(E_R) \approx \frac{e^{-E_R/18}}{1 + 0.75\,E_R}, \qquad f_{\mathrm{I}}(E_R) \approx \frac{e^{-E_R/40}}{1 + 0.65\,E_R} \tag{2.5}$$

for E_R in keV. These expressions reproduce to good accuracy the curves shown in figure 4 of [38]. Departing from eq. (2.1), the predicted spectrum in DAMA (in units of counts/kg/day/keVee) is obtained by

$$R_{\mathrm{DAMA}}(E) = \sum_{X=\mathrm{Na,I}} \frac{M_X}{M_{\mathrm{Na}} + M_{\mathrm{I}}} \left\{ [1 - f_X(E/q_X)]R_X(E/q_X) + f_X(E)R_X(E) \right\}, \tag{2.6}$$

where the first term in the curled bracket corresponds to quenched events and the second to channeled (and therefore unquenched) events.

Channeling does not occur in liquid Nobel gases like in the XENON experiment. Since no information on channeling in Germanium and Silicon is available for us, we do not take into account channeling in CDMS. Note, however, that CDMS requires the coincidence of signals in phonons and ionisation and hence, since channeled events would not give a phonon signal they would not look like a WIMP signal defined by the coincidence. Therefore, the fraction of channeled events corresponds effectively to an efficiency factor reducing the effective exposure. Hence, if channeling was indeed relevant for CDMS the final exclusion limits would be somewhat weaker.

In conclusion, channeling is an important effect for the interpretation of data from direct detection experiments and we stress the need of reliable information (probably requiring dedicated measurements) on this effect for any solid DM detector.

2.3 Fitting DAMA/LIBRA data

For the model-independent analysis of DAMA data the signal as a function of energy and time is parametrised as

$$S(E,t) = S_0(E) + A(E)\cos\omega(t - t_0), \tag{2.7}$$

with $\omega = 2\pi/1$ yr, $t_0 = 152$ day. For our analysis we use the data on the modulation amplitude $A(E)$ for the full 0.82 ton yr DAMA exposure[2] given in figure 9 of [1] in 36 bins from 2 to 20 keVee. As we will see the spectral shape of the signal is quite important for constraining the WIMP parameters. The prediction for the modulation amplitude in an energy bin i from E_i^- to E_i^+ is obtained from eq. (2.6) by

$$A_i^{\mathrm{pred}} = \int dE \frac{1}{2}[R_{\mathrm{DAMA}}(E, t=152) - R_{\mathrm{DAMA}}(E, t=335)] \int_{E_i^-}^{E_i^+} dE'G(E,E') \tag{2.8}$$

where $G(E,E')$ is a Gaussian energy resolution function with width [39]

$$\sigma_E^{\mathrm{DAMA}}/E = 0.45/\sqrt{E\,[\mathrm{keVee}]} + 0.0091. \tag{2.9}$$

---

[2]Here and in the following we use the acronym "DAMA" to denote the combined DAMA/NaI + DAMA/LIBRA data, except where explicitly noted otherwise.

Then we construct a χ^2 function

$$\chi^2_{\mathrm{DAMA}}(m_\chi, \sigma_p) = \sum_{i=1}^{36} \left(\frac{A_i^{\mathrm{pred}}(m_\chi, \sigma_p) - A_i^{\mathrm{obs}}}{\sigma_i} \right)^2, \tag{2.10}$$

using the experimental data points A_i^{obs} and their errors σ_i from figure 9 of [1].[3] We find the best fit point for the WIMP mass and the scattering cross section by minimising eq. (2.10) with respect to m_χ and σ_p. Allowed regions in the (m_χ, σ_p) plane at a given CL are obtained by looking for the contours $\chi^2(m_\chi, \sigma_p) = \chi^2_{\mathrm{min}} + \Delta\chi^2(\mathrm{CL})$, where $\Delta\chi^2(\mathrm{CL})$ is evaluated for 2 degrees of freedom (dof), e.g., $\Delta\chi^2(90\%) = 4.6$ or $\Delta\chi^2(99.73\%) = 11.8$.

In general the constant part of the spectrum, $S_0(E)$, will consist of a time-averaged dark matter contribution $\langle R \rangle$ plus an un-identified background B:

$$S_0(E) = \langle R(E) \rangle + B(E). \tag{2.11}$$

In a given model such as for example WIMP scattering, the annual modulation amplitude $A(E)$ and the averaged signal $\langle R(E) \rangle$ are not independent. Hence, for a given fit to the data on $A(E)$, the expected constant signal $\langle R(E) \rangle$ can be predicted by using eq. (2.6). In order to take this additional information into account we use the data from figure 1 of [1], which shows the constant signal S_0 in 32 energy bins from 2 to 10 keVee for the DAMA/LIBRA detectors. For each pair of (m_χ, σ_p) we calculate the expected signal from WIMP scattering $\langle R \rangle$ in each of these energy bins. Whenever $\langle R \rangle$ exceeds the observed rate in one of the bins that particular values of (m_χ, σ_p) are not consistent with the data and have to be excluded. Note that for event rates of order 1 count/kg/day/keVee and the DAMA/LIBRA exposure of 0.53 t yr statistical errors are negligible for this purpose.

2.4 Analysis of CDMS and XENON

In our analysis we include the constraints from CDMS 2005 data using Silicon (CDMS-Si) [29], which, despite the relatively low exposure of 12 kg day, provides good sensitivity to the low-mass WIMP region because of the light mass of the target nucleus ($M_{\mathrm{Si}} \simeq 26\,\mathrm{GeV}$) and the low analysis threshold of 7 keV. Furthermore, we include CDMS 2008 data on Germanium (CDMS-Ge) [3] with a threshold of 10 keV. We use the energy dependent efficiency from figure 2 of [3] which reduces the total exposure of 398.7 kg day to an effective exposure of about 121.3 kg day. For both, CDMS-Si and CDMS-Ge, no event has been observed. We calculate the expected number of events N^{pred} as a function of m_χ and σ_p by integrating eq. (2.1) over the relevant energy range and scaling with the exposure. A χ^2 is constructed using the common expression for Poisson distributed data [36], which for zero observed events simply becomes

$$\chi^2_{\mathrm{CDMS}} = 2N^{\mathrm{pred}}. \tag{2.12}$$

Exclusion contours are defined by the standard $\Delta\chi^2$ cuts for 2 dof with respect to the minimum, which of course occurs for $N^{\mathrm{pred}} = 0$. Conceptually this prescription differs from the usual way to set a limit on σ_p for fixed m_χ by requiring $N^{\mathrm{pred}} < 2.3$ for a 90% CL limit. However, by accident, since $\Delta\chi^2(90\%) = 4.6$ for 2 dof, in practice our χ^2 definition in eq. (2.12) leads to the same exclusion contour as the more conventional method of setting a limit on σ_p.

---

[3]Figure 10 of [1] shows that the A_i^{obs} are consistent with being Gaussian distributed, justifying the χ^2 adopted in eq. (2.10).

For the analysis of data from the XENON10 experiment [4] (XENON for brevity) we proceed in the following way. Using the 7 bins in nuclear recoil energy from 4.5 to 26.9 keV of table 1 of [4] the predicted number of events in bin i, $N_i^{\text{pred}}(m_\chi, \sigma_p)$ can be calculated by integrating eq. (2.1) and scaling with the exposure 316 kg day as well as the bin dependent efficiencies ϵ_c and A_{nr} given in table 1 of [4]. After the publication of ref. [4] the so called parameter $\mathcal{L}_{\text{eff}}$ relevant for the nuclear recoil energy scale in XENON was remeasured [40]. Whereas in [4] a constant value $\mathcal{L}_{\text{eff}} = 0.19$ was used, figure 3 of [40] shows an energy dependent deviation of $\mathcal{L}_{\text{eff}}$ from that value. We use the information from this figure to correct nuclear recoil energies in XENON. This leads to a somewhat higher energy threshold of about 5.5 keV (instead of 4.5), which shifts the bound on DM parameters to slightly higher values of m_χ.

XENON observes 10 candidate events whose recoil energies can be inferred from figure 3 of [4]. They are distributed over the 7 bins as $(D_i) = (1, 0, 0, 0, 3, 2, 4)$, with an expected background $(B_i) = (0.2, 0.3, 0.2, 0.8, 1.4, 1.4, 2.7)$. We use the χ^2 for Poisson distributed data [36]:

$$\chi^2_{\text{XENON}} = 2 \sum_{i=1}^{7} \left[N_i^{\text{pred}} + B_i - D_i + D_i \log \left(\frac{D_i}{N_i^{\text{pred}} + B_i} \right) \right] , \qquad (2.13)$$

where the second term in the square bracket is zero if $D_i = 0$. Again we define the exclusion curve in the (m_χ, σ_p) plane by $\Delta\chi^2(\text{CL})$ contours for 2 dof with respect to the minimum.

In both cases, CDMS and XENON we include an energy resolution of $20\%/\sqrt{E_R \, [\text{keV}]}$, and an uncertainty in the energy scale of 10%, which is added to the χ^2 definitions eqs. (2.12) and (2.13) with the help of nuisance parameters. Note that CDMS and XENON report their results directly in terms of the recoil energy already corrected by the quenching factor. In contrast to DAMA, here this is possible because only a single element is used as target.

3 Standard halo results

Figure 1 summarises our results assuming standard halo properties, showing the allowed region from DAMA together with the constraints from CDMS-Si, CDMS-Ge and XENON. First we discuss the fit to DAMA data alone (without constraints from CDMS and XENON). We find two islands in the (m_χ, σ_p) plane where DAMA can be accommodated. The best fit point is obtained at

$$m_\chi = 12 \, \text{GeV} , \quad \sigma_p = 1.3 \times 10^{-41} \, \text{cm}^2 , \qquad \chi^2_{\text{DAMA,min}} = 36.8/34 \, \text{dof} , \qquad (3.1)$$

with an excellent goodness of fit of 34%. There is also a local minimum at $m_\chi = 51 \, \text{GeV}$ with $\chi^2_{\text{local}} = 47.9$. This solution is disfavoured with respect to the best fit point at about 3σ for 2 dof ($\Delta\chi^2 = 11.1$). The allowed regions around $m_\chi \simeq 50 \, \text{GeV}$ shown in figure 1 are defined with respect to the local minimum. The low and high WIMP-mass solutions correspond to channeled and quenched scatterings on Iodine, respectively. In contrast to the situation when all events are assumed to be quenched [9], it turns out that scattering on Sodium is not relevant once channeling of Iodine events takes place. The reason is that quenched events on Sodium require a similar WIMP mass as channeled events on Iodine (i.e., $m_\chi \simeq 10 \, \text{GeV}$) but a much larger cross section σ_p (due to the A^2 dependence of the total cross section on the nucleus), and therefore, are highly suppressed once channeled scattering on Iodine takes place. In principle there would be also a solution from channeled events on Na, around $m_\chi \simeq 5 \, \text{GeV}$. However, it turns out that in this case the un-channeled events on Na still contribute to the signal, and indeed prevent fitting the data with the channeled Na events. Note that the
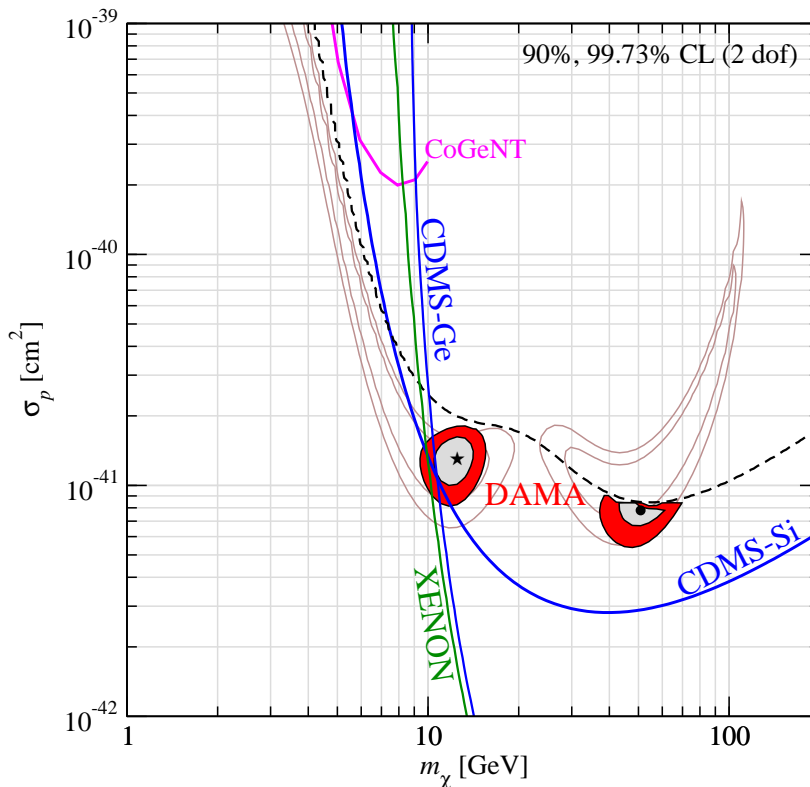
Figure 1: Allowed regions at 90% and 99.73% CL for WIMP mass and scattering cross section on nucleon for DAMA, and exclusion contours for CDMS-Si, CDMS-Ge and XENON at 90% CL. We also display the limit from CoGeNT extracted from figure 2 of [28]. The global best fit for DAMA is marked with a star, the allowed region around $m_\chi \simeq 50\,\mathrm{GeV}$ is defined with respect to the local minimum, which is marked with a dot. For DAMA we show the regions obtained from using only the modulation amplitude for 2–6 keVee (gray curves) and from using the spectral shape of the modulation signal (shaded regions). For parameters above the dashed curve the predicted number of events in DAMA/LIBRA is larger than the observed number of events.

solution around $m_\chi \simeq 50\,\mathrm{GeV}$ is excluded by some orders of magnitude by XENON and CDMS-Ge, and therefore we focus in the following on the low-mass region $m_\chi \simeq 10\,\mathrm{GeV}$.

The gray contours in figure 1 correspond to an alternative method of fitting DAMA. Instead of using the detailed spectral information of the annual modulation, we fit the time dependence of their signal integrated over energy. In figure 6 of [1] data on the residual rate $(S(t) - S_0)$ (c.f., eq. (2.7)) is given in 7 time bins of one single annual cycle. For the gray contours in figure 1 we use these data for the energy intervals 2 to 6 keVee and 6 to 14 keVee, where in the latter interval data are consistent with no annual variation. These results are very similar to the ones of [9] (if channeling is neglected, not shown in the figure) and [19] (including channeling), where only two data points for the modulation amplitude below and above 6 keVee have been used.

We observe from figure 1 that the two methods of analysing DAMA data are consistent with each other (as it should be), but also that using the spectral information gives significantly stronger constraints on the allowed region. This is illustrated in figure 2 (left), showing the 36 data points on the modulation amplitude A_i used in our default analysis. While the prediction from the best fit point of eq. (3.1) nicely follows the data (solid curve), moving
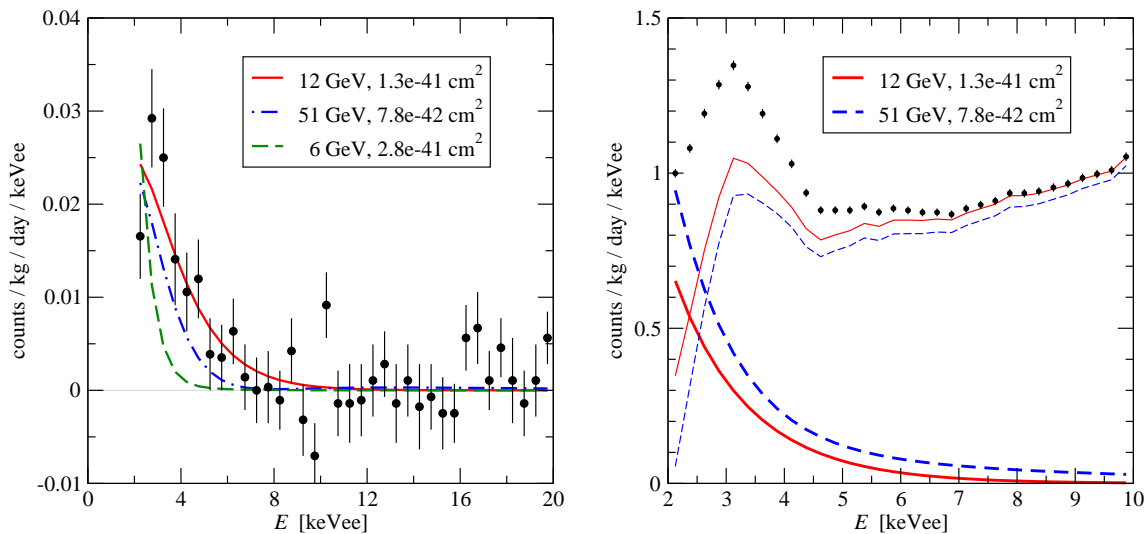
Figure 2: Left: Energy distribution of the annual modulation amplitude from DAMA/NaI and DAMA/LIBRA data extracted from figure 9 of [1] (points with error bars), together with the prediction for three examples of WIMP masses and scattering cross sections (curves). Right: Energy distribution of the time averaged rate observed in DAMA/LIBRA extracted from figure 1 of [1] (points), together with the prediction for two examples of WIMP masses and scattering cross sections (thick curves) as well as the corresponding un-identified background (thin curves). The data are corrected for the energy dependent efficiency.

to smaller WIMP masses leads to a modulation signal more peaked at the lowest energies. Therefore, although it is still possible to obtain the integrated signal in the interval from 2 to 6 keVee, the spectral shape is clearly inconsistent with data, as illustrated for $m_\chi = 6\,\mathrm{GeV}$ by the dashed curve.[4]

Finally we mention the implication of the data on the time averaged rate observed in DAMA. Parameter values above the dashed curve in figure 1 are excluded because they would lead to a higher event rate than observed. This leads to additional constraints for the high-mass solution. In figure 2 (right) we show the observed rate together with the predictions for the two local minima. Note that for the DAMA/LIBRA exposure of 0.53 t yr statistical errors are not visible at the scale of the plot. Clearly, solutions predicting a relatively large rate require that the un-identified background drops rapidly in order to give space for the WIMP signal. In particular, the solution at $m_\chi = 51\,\mathrm{GeV}$ requires that the background drops to zero in the first energy bin. Although this cannot be excluded a priori, at least such a background shape seems somewhat unlikely. The issue is less severe for the best fit point at $m_\chi = 12\,\mathrm{GeV}$, since the ratio of modulation amplitude to average rate increases for decreasing WIMP mass. However, any point close to the dashed line in figure 1 is affected by this problem.

From figure 1 we find that the parameters allowed by DAMA data at 90% CL are excluded by the 90% CL limits of CDMS-Si, CDMS-Ge, and XENON. If all data are combined

---

[4]The value for the cross section $\sigma_p = 2.8 \times 10^{-41}$ cm^2 formally gives the best fit to the data shown in figure 2 (left) for $m_\chi = 6\,\mathrm{GeV}$. However, the value required to obtain the integrated modulation amplitude for this m_χ is about a factor 2 larger, $\sigma_p = 6 \times 10^{-41}$ cm^2, as can be seen from the gray contours shown in figure 1.

by adding the individual χ^2 functions,

$$\chi^2_{\text{global}} = \chi^2_{\text{DAMA}} + \chi^2_{\text{CDMS}-\text{Ge}} + \chi^2_{\text{CDMS}-\text{Si}} + \chi^2_{\text{XENON}} , \qquad (3.2)$$

we find the minimum at $m_\chi = 9.5\,\text{GeV}$ and $\sigma_p = 1.2 \times 10^{-41}\,\text{cm}^2$ with $\chi^2_{\text{global,min}} = 59.3/(45-2)\,\text{dof}$, which corresponds to a 5% goodness of fit.

Let us note that the goodness of fit test based on $\chi^2_{\text{min}}/\text{dof}$ often is not very sensitive to tensions in the fit, especially in case of a large number of data points. This can happen if there are many data points which actually are not sensitive to the relevant parameters, and hence, allow to "hide" the problem in the fit, see for example the discussion in [41]. Because of this the goodness of fit depends also on the way of binning the data. To circumvent this weakness of the standard goodness of fit test the so-called Parameter Goodness of fit (PG) can be used [41]. Whereas the standard test measures the probability that all individual data points are fitted by an hypothesis, the PG tests the consistency of different data sets under an hypotesis. It is based on the χ^2 function

$$\chi^2_{\text{PG}} = \chi^2_{\text{global,min}} - \sum_i \chi^2_{i,\text{min}} , \qquad (3.3)$$

where $\chi^2_{\text{global,min}}$ is the χ^2 minimum of all data sets combined and $\chi^2_{i,\text{min}}$ is the minimum of the data set i. This χ^2 function measures the "price" one has to pay by the combination of the data sets compared to fitting them independently. It follows a standard χ^2 distribution and should be evaluated for the number of dof corresponding to the number of parameters in common to the data sets, see [41] for a precise definition.

To apply this method we consider the two data sets DAMA versus all the other data showing no evidence. Hence, we combine CDMS-Ge, CDMS-Si, and XENON into one data set which we denote by NEV. Then we find $\chi^2_{\text{PG}} = 22.6$. Evaluating this for 2 dof (corresponding to the two parameters m_χ and σ_p in common to both data sets) one finds that DAMA and NEV data are consistent only at a probability of 1.2×10^{-5}. This corresponds roughly to the probability of a 2.9σ fluctuation in both data sets at the same time.[5] We conclude that the explanation of DAMA results in terms of spin-independent elastic scattering of WIMPs with standard halo properties is strongly disfavoured by XENON and CDMS data. Next we investigate the stability of this result with respect to modifications of the velocity distribution of the WIMPs in the halo of our galaxy.

4 Non-standard halos

The precise limits on the cross section and mass of a dark matter candidate which are obtained from a particular observation/non-observation of a signal in a direct detection experiment depend upon the velocity dispersion of dark matter around the detector, and consequently ultimately upon astrophysical assumptions. The same set of astrophysical assumptions are normally made by different experiments so that their results can be compared with each other, the first of which being that the dark matter halo of the galaxy is an isothermal sphere

---

[5] Note that the standard $\chi^2_{\text{min}}/\text{dof}$ probability of 5% tests the fit of all individual data points at the best fit solution, whereas the PG of 1.2×10^{-5} reflects the compatibility of the DAMA and NEV data sets. These are different questions and therefore the two probabilities are consistent with each other. Our DAMA analysis is based on 36 data points on the modulation amplitude, where most of them (above 6 keVee) are always fitted perfectly, irrespectively of the disagreement with CDMS/XENON. This is an example of the above mentioned "dilution" of the standard goodness of fit test.
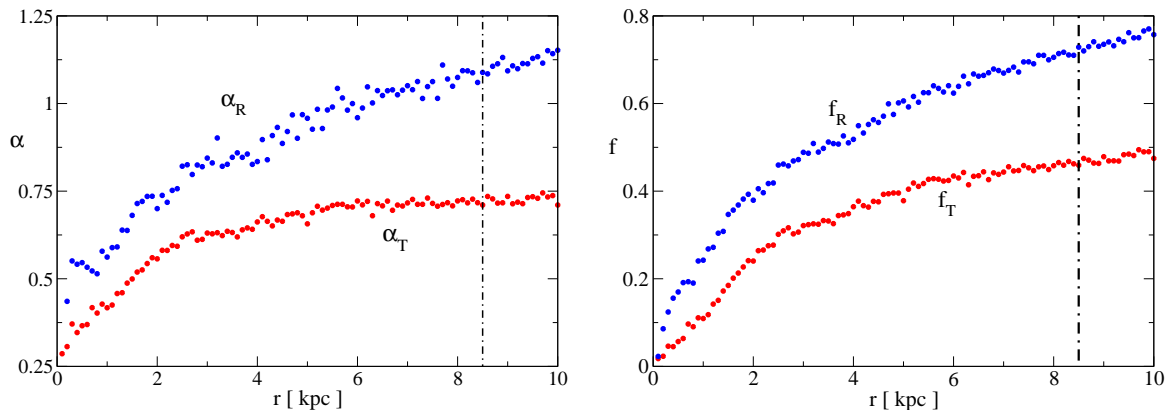
Figure 3: The parameters α_i and f_i explained in the text fitted to the radial and tangential velocity dispersions of dark matter at different radii from the centre of the Via Lactea simulation. The vertical lines indicate the position of the Sun at $r = 8.5$ kpc. The velocity dispersions are clearly non-Gaussian as one approaches the centre of the galaxy.

which means a spherically symmetric density distribution of the form $\rho \propto r^{-2}$. For such a density distribution the Keplerian velocity is independent of radius and the value of this velocity normally assumed for dark matter studies is a radius independent Keplerian velocity of 220 kms^{-1}. It is also assumed that the velocity dispersion of the dark matter profile is everywhere isotropic and Gaussian, the width of the Gaussian distribution corresponding to the Keplerian velocity of the profile. It turns out that we do not actually expect any of these assumptions to hold true for a realistic dark matter halo.

Over the past decade, N-body simulations of increasingly large numbers of dark matter particles have allowed us to obtain more information about the kind of dark matter halos that one would expect to form in an expanding universe (see e.g. [42]). These simulations show that one might expect a dark matter density that decreases more steeply with radius at large radii rather than have the same power law at all radii as in an isothermal profile [43]. Furthermore, the orbits taken by dark matter particles in a realistic simulation are usually rather radial, resulting in an anisotropic velocity dispersion [44].

Note that one can also obtain an anisotropic velocity dispersion in a halo where the density distribution is not spherically symmetric, but rather triaxial as in [32]. In this work however, we only consider dark matter halos where the density distribution is spherically symmetric although the velocity dispersion does not have to be. Also, in a non-extensive ideal gas where there is a long range attractive force between the particles such as we have here in the form of gravity, one generically expects deviations from Gaussian velocity distribution [33]. Furthermore, if the dark matter is still not completely virialised but is still coming into equilibrium, there will be a superposition of multiple dark matter populations at any given place in the halo. This effect would also lead to deviations from a Gaussian distribution of velocities.

In 2006, the results from a Milky Way size dark matter halo simulation called Via Lactea containing 234 million particles were published [34]. We have looked at this data to see how much the dark matter distribution experienced by an observer at the Solar radius within this simulation would vary from the normal assumptions stated above for observers on Earth. For each particle in the simulation there is a position vector x_i and velocity vector v_i, plus the local gravitational potential per unit mass in units of velocity squared $U(x_i)$. We express

the velocities in terms of the square root of their local potential $\tilde{v}_i = v_i/\sqrt{-U(x_i)}$. Next we work out the angle between the radial direction and the overall velocity vector. We then use this to decompose the velocity into a radial part and a part perpendicular to that which we call tangential. For each radius we bin the tangential and the radial velocities obtaining two distributions. We fit the one dimensional radial distribution using the following expression which we find to be a better fit than the Tsallis distributions (designed to fit non-extensive or multiple temperature distributions) used in [33]

$$\frac{1}{N_R} \exp \left[- \left(\frac{\tilde{v}_R^2}{f_R^2} \right)^{\alpha_R} \right] . \tag{4.1}$$

Because we have rescaled the velocities with respect to $\sqrt{-U(x_i)}$, f_R and α_R are dimensionless constants of order one. The naive assumption is that the width of the velocity distribution at a given radius is simply the Keplerian velocity at that radius. While information about the mass distribution of dark matter is required to go from the potential to the Keplerian velocity, The parameter f_R is an indication of how badly this assumption is broken. α encodes the deviation from Gaussianity ($\alpha = 1$ corresponding to a Gaussian). For the one dimensional case, the normalisation is analytic, $N_R = 2 f_R \Gamma(1 + 1/2\alpha_R)$. We perform the same fitting procedure for the tangential velocity, fitting

$$\frac{2\pi v_T}{N_T} \exp \left[- \left(\frac{\tilde{v}_T^2}{f_T^2} \right)^{\alpha_T} \right] \tag{4.2}$$

and while we are not aware of an analytic expression for N_T it is trivial to obtain it numerically. Note, in terms of the two dimensions perpendicular to the radial direction R, $\tilde{v}_T^2 = \tilde{v}_\theta^2 + \tilde{v}_\phi^2$.

Using the data from the Via Lactea simulation, we have fitted for values of f_i and α_i as a function of radius from the centre of the galaxy. The results, which can be seen in figure 3, show that there is a considerable deviation from Gaussianity in the velocity dispersion of the galaxy. Both the deviation from Gaussianity, the anisotropy of the velocity dispersion and the change in the relationship between the width of the dispersion and the local Keplerian velocity will change the ratio between the expected modulation in the DAMA experiment and the total expected events at XENON and CDMS. We have calculated these changes and attempted to see if they can increase the likelihood of the results from both experiments being compatible, the results of the new fits can be seen in figure 4(a).

It turns out that the deviation from the assumptions of the isothermal sphere which are predicted by the Via Lactea simulation are not sufficient to bring the region in parameter space favoured by DAMA away from the region disfavoured by XENON and CDMS. The numbers associated with these regions are provided in table 1 and show that using the velocity dispersion predicted by Via Lactea leads to only a very small reduction in χ^2 and the goodness of fit is still unacceptably small.

It is therefore interesting to ask what kind of halo parameters could lead to a better fit to the data, and how realistic would such parameters be? There are examples in the literature of the use of a stream of dark matter to boost the annual modulation signal [9]. In this work, we choose to retain the spherical symmetry of the halo density and instead of adding a stream, vary both the width of the velocity dispersion and the anisotropy parameter β_{vel} defined as

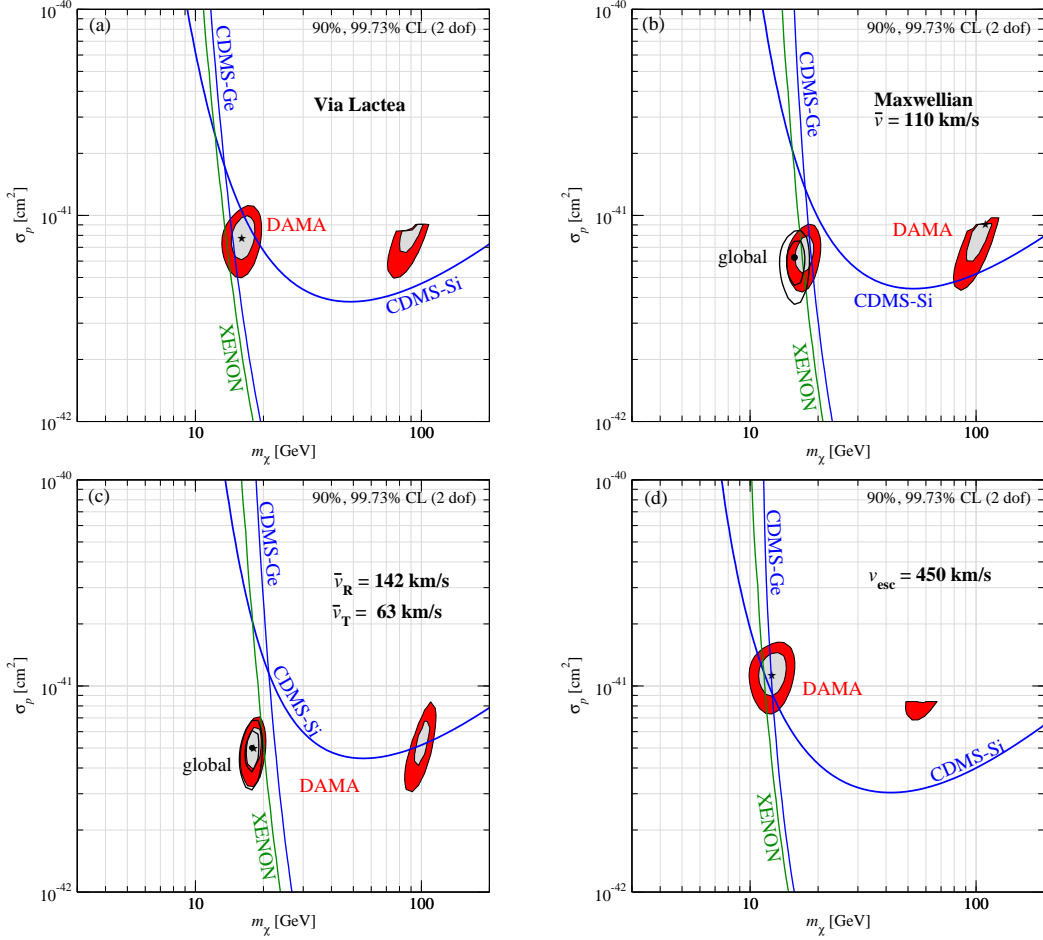$$\beta_{\text{vel}} = 1 - \frac{\bar{v}_T^2}{\bar{v}_R^2} . \tag{4.3}$$

Figure 4: Allowed regions at 90% and 99.73% CL for DAMA, and exclusion contours for CDMS-Si, CDMS-Ge and XENON at 90% CL for the DM halo obtained in the Via Lactea simulation (a), an isotropic Maxwellian halo with dispersion $\bar{v} = 110$ km/s (b), an asymmetric Maxwellian halo with dispersion $\bar{v}_R = 142$ km/s in the radial direction and $\bar{v}_T = 63$ km/s in the tangential direction (c), and an isotropic Maxwellian halo with dispersion $\bar{v} = 220$ km/s and escape velocity $v_{\rm esc} = 450$ km/s (d). The best fit for DAMA is marked with a star. In the panels (b) and (c) we show also the 90% and 99.73% CL regions for the global data combining all experiments, as well as the global best fit point (marked with a dot).

halo model	$\chi^2_{\rm DAMA,min}$	$m^{\rm DAMA}_{\chi,\rm best}$	$\chi^2_{\rm glob,min}$	GOF	$\chi^2_{\rm PG}$	PG	$m^{\rm glob}_{\chi,\rm best}$
default analysis	36.8	12	59.3	0.05	22.6	1×10^{-5}	9.5
Via Lactea simulation	35.1	16	56.7	0.08	21.6	2×10^{-5}	13.9
Maxwellian $\bar{v} = 110 \, {\rm km/s}$	32.9	108	46.8	0.32	13.5	1×10^{-3}	16
$\bar{v}_R = 142 \, {\rm km/s}$, $\bar{v}_T = 63 \, {\rm km/s}$	32.7	18	39.6	0.62	6.5	0.04	18
$v_{\rm esc} = 450 \, {\rm km/s}$	36.5	12	51.6	0.17	15.1	5×10^{-4}	11

Table 1: Summary of the fits to DAMA data and global data (DAMA, CDMS-Ge, CDMS-Si, XENON) for different WIMP halos. We give the best fit χ^2 values, the goodness of fit (assuming 43 dof), the PG testing the consistency of DAMA with all other data, as well as the best fit WIMP masses (in GeV).

A reduction in the width of the velocity dispersion of dark matter alone helps reconcile the two data sets without the need to introduce anisotropy. If we assume an isotropic distribution of dark matter ($\beta_{\mathrm{vel}} = 0$) and reduce $\bar{v}$ to 110 km/s which is half of the Keplerian velocity at the solar radius, the goodness of fit increases dramatically (see table 1). A further improvement in the fit is made if one assumes a velocity dispersion lower than Keplerian, but also highly anisotropic such that $\bar{v}_R = 142$ km/s and $\bar{v}_T = 63$ km/s. As visible in figure 4 (c) in this cases the entire 90% CL region of DAMA is consistent with the 90% CL bounds from CDMS and XENON. For the asymmetric velocity distribution the global χ^2 drops by about 20 units compared to the default analysis and provides an excellent goodness of fit of 62%. The PG test gives compatibility of DAMA with NEV data with a probability of 4%, due to the remaining constraint from XENON.

A valid question is then whether such low and anisotropic values of the velocity dispersions are at all realistic. In order to check on the feasibility of such values, one needs to think about particular dark matter halos and see if the solutions of the (Maxwell-) Jeans equations allow simultaneously both a high velocity anisotropy ($\beta_{\mathrm{vel}} \sim 0.8$) and low velocity distribution at the location of the Sun.

In order to solve the Jeans equations, we will need to understand the distribution of mass in the galaxy. Integration of a spherically symmetric dark matter profile with a well defined functional form is trivial. However, at the radius of the Sun, it is important to consider not only dark matter but also the presence of baryons, which make up most of the mass in the central regions of the galaxy. To model the Milky Way baryon density we assume cylindrical symmetry and ignore any spiral arms or bars. For the central bulge of stars we assume a density of the form $\rho \propto r^{-\gamma} e^{-r/\lambda}$ while for the disk we assume a (Kuzmin) delta function of matter in the z direction (z is the coordinate perpendicular to the disk) with a surface density $\sigma_{\mathrm{disk}}(r) = \frac{cM_{\mathrm{disk}\infty}}{2\pi(r^2+c^2)^{\frac{3}{2}}}$. We choose the parameters of the model to match observations of the Milky Way: $\gamma = 1.85$, $\lambda = 1\,\mathrm{kpc}$, $c = 5\,\mathrm{kpc}$ and with the total disk and bulge mass $M_{\mathrm{disk}\infty} = 5M_{\mathrm{bulge}} = 6.5 \times 10^{10} M_{\odot}$ [45–48]. We assume that the disk comes to an end at a radius of 15 kpc.

In order to parametrise our dark matter density profile we will consider a profile which assumes two asymptotic radial power law behaviors at both small (γ) and large (β) radii.[6] In this profile, known as the '$\alpha\beta\gamma$' profile (or the Zhao profile), the density as a function of radius is given by the expression

$$\rho(r) = \frac{\rho_0}{(r/a)^{\gamma}\left[1 + (r/a)^{\alpha}\right]^{\frac{\beta-\gamma}{\alpha}}} \tag{4.4}$$

where α governs the radial rate at which the profile interpolates between the asymptotic powers $-\gamma$ and $-\beta$. The parameter a is a characteristic scale radius determining the location dividing the two regions described by a single power law.

Having assumed a value for α, β, γ and a we then solve for ρ_0 in order to get the correct value of the Keplerian velocity at the solar radius. This also determines the location of the virial radius r_{vir} which in this work is defined to be the radius of the sphere within which the average density is 250 times the critical density of the universe (we assume $h = 0.7$). The ratio between r_{vir} and a is referred to as the concentration of the dark matter halo.

---

[6]This β in the density profile should not be confused with the velocity dispersion anisotropy parameter β_{vel}.
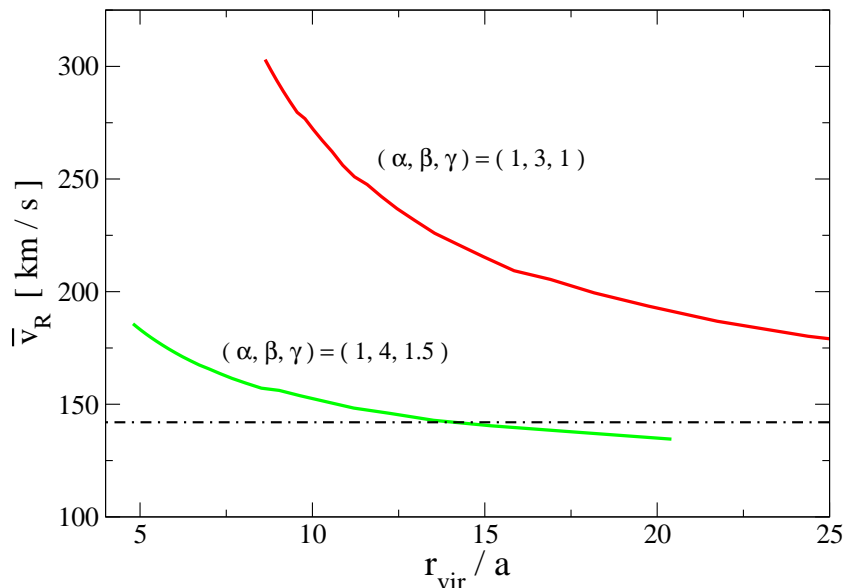
Figure 5: Here we plot the radial velocity dispersion $\bar{v}_R$ at the solar radius $r = 8.5$ kpc as a function of the concentration of the dark matter halo $r_{\rm vir}/a$ for two different dark matter profiles. We have assumed that the velocity dispersion anisotropy parameter $\beta_{\rm vel} = 0.8$ and is a constant with respect to radius. The horizontal line corresponds to the value of $\bar{v}_R$ which helps explain the discrepancy. It appears that only for sets of halo parameters such as $(\alpha, \beta, \gamma) = (1, 4, 1.5)$ can one reconcile such a high value of β with a low enough radial velocity dispersion to help explain the discrepancy between DAMA and XENON/CDMS.

Once we are in possession of these parameters, we can proceed to solve the Jeans equation for the radial velocity dispersion [49]

$$\frac{1}{\rho}\frac{d\left(\rho\bar{v}_R^2\right)}{dr} + \frac{2\beta_{\rm vel}\bar{v}_R^2}{r} = -\frac{d\phi}{dr} = -\frac{V_c^2}{r}\,, \tag{4.5}$$

where $\phi(r)$ and $V_c(r)$ are the potential and Keplerian velocity at a given radius. We integrate this equation inwards from a large radius several times the magnitude of $r_{\rm vir}$ where we assume that $\rho\bar{v}_R^2 = 0$. We have checked that the result at $r = 8.5$ kpc is independent of the exact radius at which this boundary condition is applied. We have also assumed that, in the absence of a better approximation, the anisotropy parameter $\beta_{\rm vel}$ is a constant throughout the halo.

The results are plotted in figure 5 and show that for a NFW profile where the parameters are chosen such that $(\alpha, \beta, \gamma) = (1, 3, 1)$ it seems to be rather difficult to imagine that such a large value of the velocity anisotropy $\beta_{\rm vel}$ could be consistent with low enough values of the velocity dispersion to match the data. We also look at a non-standard halo with $(\alpha, \beta, \gamma) = (1, 4, 1.5)$. The inner slope of such a halo is quite steep, but even larger values of γ than this may be expected in dark matter halos where adiabatic contraction due to the presence of baryons has occurred [44]. The rate at which density decreases at larger radii is also larger than what is normally assumed.

If we are willing to accept such parameters for the dark matter profile, it seems that the highly anisotropic value of $\beta_{\rm vel} \sim 0.8$ that we require as one ingredient to make the DAMA data more consistent with XENON and CDMS is not completely inconsistent with the very low velocity dispersions that form the other ingredient. The analysis presented here is meant

only as a suggestion of the magnitude of possible effects. If such explanations of the DAMA data were to be taken seriously, a much deeper analysis of the Jeans equations should be undertaken.

Finally we mention that if one assumes a very low dark matter escape velocity at the solar radius then one would remove many of the fastest moving dark matter particles which would leave the halo. This would also result in more accord between DAMA and other experiments but obtaining a large enough effect is difficult — as expressed in table 1, lowering the escape velocity to 450 km/s would only marginally make the fit more acceptable. This, however, must be considered an unrealistic solution, since the escape velocity at the Solar radius is already 440 km/s even if there were no more matter in the Galaxy at larger radii.

To summarise this section, it seems that without the use of streams but rather by considering highly anisotropic velocity dispersions with magnitudes far below the local Keplerian velocity at the radius of the Sun would it be possible to reduce the conflict between DAMA and XENON/CDMS.

5 Conclusions

Prompted by recent results from DAMA/LIBRA which establish the annual modulation of their event rate at the 8.2σ level, we have studied the interpretation of this signal in terms of spin-independent elastic WIMP scattering. We have shown that the energy spectrum of the modulation signal strongly restricts the region of WIMP masses below 10 GeV, confining WIMP masses consistent with the DAMA data close to $m_\chi \simeq 12$ GeV. This region is excluded by the limits from CDMS and XENON, and therefore we conclude that even if channeling is taken into account this interpretation of the DAMA modulation signal is disfavoured. Applying a stringent test to evaluate the consistency of DAMA with null-result experiments we find consistency only with a formal probability of 10^{-5}.

We have studied how robust this result is with respect to variations of the WIMP velocity distribution in our galaxy by changing various parameters of the distribution function. We find that decreasing the dispersion of the distribution can somewhat reduce the tension in the fit. Adopting in addition an asymmetric WIMP velocity profile with a larger dispersion in the radial direction than tangential improves the fit considerably. We conclude that in principle it is possible to reconsile DAMA in the considered framework, at the price of rather exotic properties of the DM halo. The question remains whether such halo properties can be realistic at all. We have checked that a WIMP velocity distribution based on the Via Lactea N-body dark matter simulation does not improve the fit considerably with respect to the standard Maxwellian halo model.

Finally we mention that the negative conclusion on the compatibility of DAMA with CDMS and XENON relies crucially on the energy threshold of the latter two. In particular, a shift in the nuclear recoil energy scale in these experiments may change the conclusion. Indeed, the new measurements of the $\mathcal{L}_{\mathrm{eff}}$ parameter in XENON [40] (which has not been implemented in the first arXiv version of this work) made the disagreement between DAMA and XENON somewhat less sever.

Acknowledgments

	$\chi^2_{\mathrm{DAMA,min}}$	$m^{\mathrm{DAMA}}_{\chi,\mathrm{best}}$	$\chi^2_{\mathrm{glob,min}}$	GOF	χ^2_{PG}	PG	$m^{\mathrm{glob}}_{\chi,\mathrm{best}}$
default analysis	36.8	12	59.3	0.05	22.6	1×10^{-5}	9.5
double σ_E^{DAMA}	37.9	11	52.1	0.16	14.3	8×10^{-4}	9.0
w/o 1$^{\mathrm{st}}$ DAMA data point	30.3	10	44.4	0.37	14.1	9×10^{-4}	8.6

Table 2: Summary of fits to DAMA data and global data (DAMA, CDMS-Ge, CDMS-Si, XENON) for the two ad-hoc modifications of the DAMA analysis of figure 6. We give the best fit χ^2 values, the goodness of fit (assuming 42 dof for the last row and 43 dof otherwise), the PG testing the consistency of DAMA with all other data, as well as the best fit WIMP masses (in GeV).
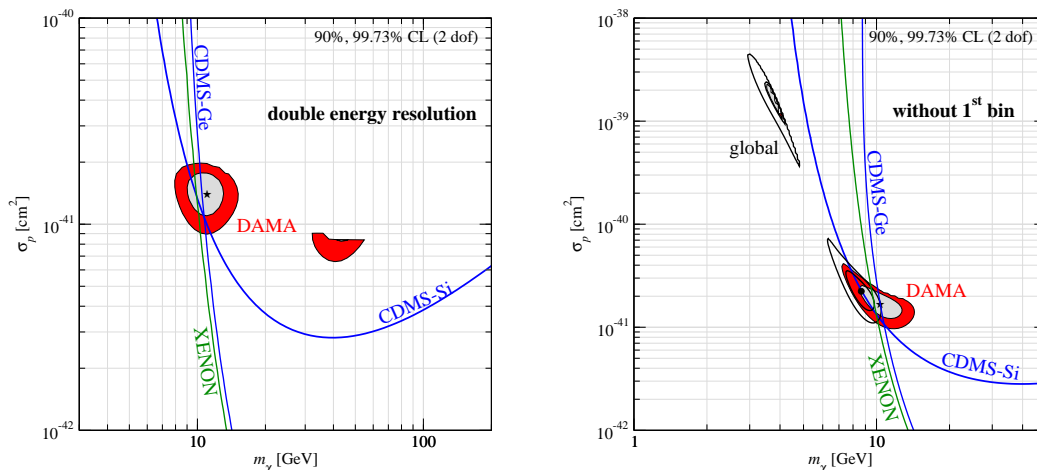

Figure 6: Allowed regions at 90% and 99.73% CL for DAMA, and exclusion contours for CDMS-Si, CDMS-Ge and XENON at 90% CL for two ad-hoc modifications of the DAMA analysis. Left: we artificially assume an energy resolution in DAMA a factor two worse than the value given in [39]. Right: omitting the lowest energy bin of the annual modulation spectrum between 2 and 2.5 keVee. The best fit for DAMA is marked with a star. In the right panel we show also the 90% and 99.73% CL regions for the global data combining all experiments, as well as the global best fit point (marked with a dot).

A   Comments on the DAMA spectral information

Our results are largely based on the fact that DAMA spectral information excludes the low-mass WIMP region below 10 GeV. Obviously any effect which affects the spectral shape of the signal will have an impact on this conclusion. First, the smearing due to the energy resolution of the detector is important. We have checked this by artificially increasing the width of the energy resolution function given in eq. (2.9) [39] by a factor of two. The global fit improves by roughly 7 units in χ^2, but the tension between DAMA and NEV data persists at the level of 8×10^{-4}, compare table 2 and figure 6 (left).

From figure 2 (left) it follows that the somewhat low data point in the first energy bin is very important in constraining the WIMP mass. We have repeated the analysis by excluding this bin from the fit, using only the data on the modulation signal above 2.5 keVee. In this case the DAMA allowed region extends to lower values of the WIMP mass, and

once the NEV data are added the globally allowed region includes values of $m_\chi \sim 4\,\text{GeV}$ and $\sigma_p \sim 10^{-39}\,\text{cm}^2$ at 90% CL. This region originates from channeled events on Sodium which now can accommodate the spectrum without the first bin, despite the contribution of un-channeled Na events. Let us note, however, that in this region constraints from other experiments, like CRESST-I [25], TEXONO [27], or CoGeNT [28] are relevant. The global best fit point has an excellent $\chi^2_{\text{glob,min}} = 44.4/42$ dof.[7]

Furthermore, we remark that any systematical uncertainty affecting the low energy spectrum may be relevant. For example, figure 26 of [39] shows that the efficiency for DAMA single-hit events starts to deviate from 1 below about 8 keVee, just in the signal region. Therefore, a possible uncertainty on this low energy efficiency may affect the exclusion of the light WIMP region. In the absence of detailed information on possible energy-dependent systematic uncertainties we neglect such effects in our analysis. Let us note that the *ratio* of the signals in June and December would be less affected by systematics, since any multiplicative uncertainty (even energy dependent) would cancel, whereas the rate *difference* published by the DAMA collaboration is affected by such uncertainties.

Finally, we mention that the so-called Migdal effect could lead to modifications of the predicted energy spectrum in DAMA, see [50] for a discussion and references. An investigation of this effect is beyond the scope of this work.

B   Comparison with other studies

In this appendix we compare the results of our work to some studies from other authors. The authors of [19] come to a positive conclusion on the consistency between DAMA and constraints from other experiments, since they do not include the information on the spectral shape of the DAMA signal. In a work which appeared after ours on the preprint server [51], the same authors performed also an analysis including the spectrum which is in agreement with our results.

Our work appeared on the preprint server basically at the same time as [52], with similar results. As in our study these authors emphasize the importance of the spectral information of the DAMA annual modulation and the constraint from the total unmodulated rate. Whereas [52] discusses DM streams, our work considers non-standard halo models.

A similar study has been performed in [53], stressing also the relevance of spectral information and extending the analysis to spin-dependent cross sections. The general results for the spin-independent case are in quantitative agreement with us, though in some cases the authors draw different conclusions. In particular, they use a variety of statistical tests complementary to ours. Whereas our methods are largely based on parameter estimation ($\Delta\chi^2$ values with respect to the best fit point), these authors show also contours of probabilities from a goodness-of-fit test based on absolute χ^2 values. As mentioned at the end of section 3 this method is often not very sensitive to a tension between different data sets, see also footnote 5. Furthermore, by showing contours up to the 5 and even 7σ CL they do find overlap regions. Let us also comment on the best fit point for DAMA, obtained at $m_\chi = 80\,\text{GeV}$ in table IV of [53], compared to our result $m_\chi = 12\,\text{GeV}$ from eq. (3.1). The reason why we disfavour the fit in the large DM mass region is the inclusion of the constraint from the un-

---

[7]The improvement of the consistency of NEV and DAMA data is only partially visible in the PG value of about 0.1%, which is still rather low. The reason is that also the fit of DAMA alone improves from $\chi^2_{\text{DAMA,min}} = 36.8$ to 30.3 by dropping the first bin, which compensates partially the improvement in the global fit.

modulated rate in DAMA, which cuts away large part of this region, including also the best fit point of [53], compare figure 1, and shifts the global best fit point to the low mass region.

References

[1] DAMA collaboration, R. Bernabei et al., *First results from DAMA/LIBRA and the combined results with DAMA/NaI*, *Eur. Phys. J.* **C 56** (2008) 333 [arXiv:0804.2741] [SPIRES].

[2] G. Jungman, M. Kamionkowski and K. Griest, *Supersymmetric dark matter*, *Phys. Rept.* **267** (1996) 195 [hep-ph/9506380] [SPIRES].

[3] CDMS collaboration, Z. Ahmed et al., *A search for WIMPs with the first five-tower data from CDMS*, arXiv:0802.3530 [SPIRES].

[4] XENON collaboration, J. Angle et al., *First results from the XENON10 dark matter experiment at the Gran Sasso national laboratory*, *Phys. Rev. Lett.* **100** (2008) 021303 [arXiv:0706.0039] [SPIRES].

[5] P. Ullio, M. Kamionkowski and P. Vogel, *Spin dependent WIMPs in DAMA?*, *JHEP* **07** (2001) 044 [hep-ph/0010036] [SPIRES].

[6] C. Savage, P. Gondolo and K. Freese, *Can WIMP spin dependent couplings explain DAMA data, in light of null results from other experiments?*, *Phys. Rev.* **D 70** (2004) 123513 [astro-ph/0408346] [SPIRES].

[7] A. Bottino, F. Donato, N. Fornengo and S. Scopel, *Lower bound on the neutralino mass from new data on CMB and implications for relic neutralinos*, *Phys. Rev.* **D 68** (2003) 043506 [hep-ph/0304080] [SPIRES].

[8] A. Bottino, F. Donato, N. Fornengo and S. Scopel, *Light neutralinos and WIMP direct searches*, *Phys. Rev.* **D 69** (2004) 037302 [hep-ph/0307303] [SPIRES].

[9] P. Gondolo and G. Gelmini, *ComPatibility of DAMA dark matter detection with other searches*, *Phys. Rev.* **D 71** (2005) 123520 [hep-ph/0504010] [SPIRES].

[10] R. Bernabei et al., *Investigating pseudoscalar and scalar dark matter*, *Int. J. Mod. Phys.* **A 21** (2006) 1445 [astro-ph/0511262] [SPIRES].

[11] M. Pospelov, A. Ritz and M.B. Voloshin, *Bosonic super-WIMPs as keV-scale dark matter*, *Phys. Rev.* **D 78** (2008) 115012 [arXiv:0807.3279] [SPIRES].

[12] P. Gondolo and G. Raffelt, *Solar neutrino limit on the axion-like interpretation of the DAMA signal*, arXiv:0807.2926 [SPIRES].

[13] R. Bernabei et al., *Investigating electron interacting dark matter*, *Phys. Rev.* **D 77** (2008) 023506 [arXiv:0712.0562] [SPIRES].

[14] D. Tucker-Smith and N. Weiner, *Inelastic dark matter*, *Phys. Rev.* **D 64** (2001) 043502 [hep-ph/0101138] [SPIRES].

[15] S. Chang, G.D. Kribs, D. Tucker-Smith and N. Weiner, *Inelastic dark matter in light of DAMA/LIBRA*, arXiv:0807.2250 [SPIRES].

[16] R. Foot, *Mirror dark matter and the new DAMA/LIBRA results: a simple explanation for a beautiful experiment*, *Phys. Rev.* **D 78** (2008) 043529 [arXiv:0804.4518] [SPIRES].

[17] A. Bottino, F. Donato, N. Fornengo and S. Scopel, *Zooming in on light relic neutralinos by direct detection and measurements of galactic antimatter*, *Phys. Rev.* **D 77** (2008) 015002 [arXiv:0710.0553] [SPIRES].

[18] A. Bottino, F. Donato, N. Fornengo and S. Scopel, *Interpreting the recent results on direct search for dark matter particles in terms of relic neutralino*, *Phys. Rev.* **D 78** (2008) 083520 [arXiv:0806.4099] [SPIRES].

[19] F. Petriello and K.M. Zurek, *DAMA and WIMP dark matter*, *JHEP* **09** (2008) 047 [arXiv:0806.3989] [SPIRES].

[20] J.L. Feng, J. Kumar and L.E. Strigari, *Explaining the DAMA signal with WIMPless dark matter*, *Phys. Lett.* **B 670** (2008) 37 [arXiv:0806.3746] [SPIRES].

[21] E.M. Drobyshevski, *Channeling effect and improvement of the efficiency of charged particle registration with crystal scintillators*, *Mod. Phys. Lett.* **A 23** (2008) 3077 [arXiv:0706.3095] [SPIRES].

[22] A. Bottino, N. Fornengo and S. Scopel, *Light relic neutralinos*, *Phys. Rev.* **D 67** (2003) 063519 [hep-ph/0212379] [SPIRES].

[23] V. Barger, P. Langacker and H.-S. Lee, *Lightest neutralino in extensions of the MSSM*, *Phys. Lett.* **B 630** (2005) 85 [hep-ph/0508027] [SPIRES].

[24] J.F. Gunion, D. Hooper and B. McElrath, *Light neutralino dark matter in the NMSSM*, *Phys. Rev.* **D 73** (2006) 015011 [hep-ph/0509024] [SPIRES].

[25] **CRESST-I** collaboration, M.F. Altmann et al., *Results and plans of the CRESST dark matter search*, astro-ph/0106314 [SPIRES].

[26] CDMS collaboration, D.S. Akerib et al., *New results from the Cryogenic Dark Matter Search experiment*, *Phys. Rev.* **D 68** (2003) 082002 [hep-ex/0306001] [SPIRES].

[27] TEXONO collaboration, S.T. Lin et al., *New limits on spin-independent couplings of low-mass WIMP dark matter with a germanium detector at a threshold of* 200 *eV*, arXiv:0712.1645 [SPIRES].

[28] CoGeNT collaboration, C.E. Aalseth et al., *Experimental constraints on a dark matter origin for the DAMA annual modulation effect*, *Phys. Rev. Lett.* **101** (2008) 251301 [arXiv:0807.0879] [SPIRES].

[29] CDMS collaboration, D.S. Akerib et al., *Limits on spin-independent WIMP nucleon interactions from the two-tower run of the Cryogenic Dark Matter Search*, *Phys. Rev. Lett.* **96** (2006) 011302 [astro-ph/0509259] [SPIRES].

[30] P. Belli, R. Cerulli, N. Fornengo and S. Scopel, *Effect of the galactic halo modeling on the DAMA/NaI annual modulation result: an extended analysis of the data for WIMPs with a purely spin-independent coupling*, *Phys. Rev.* **D 66** (2002) 043503 [*Erratum ibid.* **D 69** (2004) 109902] [hep-ph/0203242] [SPIRES].

[31] N. Fornengo and S. Scopel, *Temporal distortion of annual modulation at low recoil energies*, *Phys. Lett.* **B 576** (2003) 189 [hep-ph/0301132] [SPIRES].

[32] A.M. Green, *Effect of halo modelling on WIMP exclusion limits*, *Phys. Rev.* **D 66** (2002) 083003 [astro-ph/0207366] [SPIRES].

[33] J.D. Vergados, S.H. Hansen and O. Host, *The impact of going beyond the Maxwell distribution in direct dark matter detection rates*, *Phys. Rev.* **D 77** (2008) 023509 [arXiv:0711.4895] [SPIRES].

[34] J. Diemand, M. Kuhlen and P. Madau, *Dark matter substructure and gamma-ray annihilation in the Milky Way halo*, *Astrophys. J.* **657** (2007) 262 [astro-ph/0611370] [SPIRES].

[35] G. Gelmini and P. Gondolo, *WIMP annual modulation with opposite phase in late-infall halo*

models, *Phys. Rev.* **D 64** (2001) 023504 [`hep-ph/0012315`] [SPIRES].

[36] PARTICLE DATA GROUP collaboration, W.M. Yao et al., *Review of particle physics*, *J. Phys.* **G 33** (2006) 1 [SPIRES].

[37] A.M. Green, *Effect of realistic astrophysical inputs on the phase and shape of the WIMP annual modulation signal*, *Phys. Rev.* **D 68** (2003) 023004 [*Erratum ibid.* **D 69** (2004) 109902] [`astro-ph/0304446`] [SPIRES].

[38] R. Bernabei et al., *Possible implications of the channeling effect in NaI(Tl) crystals*, *Eur. Phys. J.* **C 53** (2008) 205 [`arXiv:0710.0288`] [SPIRES].

[39] DAMA collaboration, R. Bernabei et al., *The DAMA/LIBRA apparatus*, *Nucl. Instrum. Meth.* **A 592** (2008) 297 [`arXiv:0804.2738`] [SPIRES].

[40] P. Sorensen et al., *The scintillation and ionization yield of liquid xenon for nuclear recoils*, `arXiv:0807.0459` [SPIRES].

[41] M. Maltoni and T. Schwetz, *Testing the statistical compatibility of independent data sets*, *Phys. Rev.* **D 68** (2003) 033020 [`hep-ph/0304176`] [SPIRES].

[42] V. Springel et al., *Simulating the joint evolution of quasars, galaxies and their large-scale distribution*, *Nature* **435** (2005) 629 [`astro-ph/0504097`] [SPIRES].

[43] J.F. Navarro, C.S. Frenk and S.D.M. White, *The structure of cold dark matter halos*, *Astrophys. J.* **462** (1996) 563 [`astro-ph/9508025`] [SPIRES].

[44] M. Gustafsson, M. Fairbairn and J. Sommer-Larsen, *Baryonic pinching of galactic dark matter haloes*, *Phys. Rev.* **D 74** (2006) 123522 [`astro-ph/0608634`] [SPIRES].

[45] H. Zhao, *A self-consistent dynamical model for the COBE detected galactic bar*, `astro-ph/9512064` [SPIRES].

[46] W. Dehnen and J. Binney, *Mass models of the Milky Way*, *Mon. Not. Roy. Astron. Soc.* **294** (1998) 429 [`astro-ph/9612059`] [SPIRES].

[47] A. Klypin, H. Zhao and R.S. Somerville, *ΛCDM-based models for the Milky Way and M31 I: dynamical models*, *Astrophys. J.* **573** (2002) 597 [`astro-ph/0110390`] [SPIRES].

[48] S.M. Kent, T.M. Dame and G. Fazio, *Galactic structure from the spacelab infrared telescope. 2. Luminosity models of the Milky Way*, *Astrophys. J.* **378** (1991) 131 [SPIRES].

[49] J. Binney and S. Tremaine, *Galactic dynamics*, Princeton University Press, Princeton U.S.A. (1987).

[50] R. Bernabei et al., *On electromagnetic contributions in WIMP quests*, *Int. J. Mod. Phys.* **A 22** (2007) 3155 [`arXiv:0706.1421`] [SPIRES].

[51] D. Hooper, F. Petriello, K.M. Zurek and M. Kamionkowski, *The new DAMA Dark-Matter Window and Energetic-neutrino searches*, `arXiv:0808.2464` [SPIRES].

[52] S. Chang, A. Pierce and N. Weiner, *Using the energy spectrum at DAMA/LIBRA to probe light dark matter*, `arXiv:0808.0196` [SPIRES].

[53] C. Savage, G. Gelmini, P. Gondolo and K. Freese, *compatibility of DAMA/LIBRA dark matter detection with other searches*, `arXiv:0808.3607` [SPIRES].